Modeling the Axial Crush Response of CFRP Tubes using MAT054, MAT058 and MAT262 in LS-DYNA®

Aleksandr Cherniaev, John Montesano, Clifford Butcher
Department of Mechanical & Mechatronics Engineering, University of Waterloo, 200 University Ave. West, Waterloo N2L 3G1, Canada

Abstract

Predictive capabilities of three LS-DYNA composite material models – MAT054, MAT058 and MAT262 – were investigated and compared with respect to modeling of axial crushing of CFRP energy absorbers. Results of crush simulations with non-calibrated material models were compared with available experimental data, and then parameter tuning was conducted to improve correlation with experiments. Furthermore, calibrated material models were used to conduct independent crash simulations with a distinct composite layup. Simulations with calibrated MAT054 predicted axial crush response of the energy absorbers with a reasonable accuracy. MAT058 was found to be intrinsically less accurate in predicting the peak force due to its inability to account for reduction of longitudinal compressive strength of a ply in the case of transverse compressive failure. It was also found that simulations with pre-calibrated MAT058 can predict non-physical failure modes, such as e.g. global buckling instead of stable axial crushing. Owing to complexity of its constitutive model, MAT262 required extensive calibration before a satisfactory agreement with experimental data could be achieved, which constitutes the major limitation of this material model. Instead of simple trial and error approach employed for other models, it was found more practical to use response surface approximation and gradient optimization in order to tune the parameters of MAT262.

1. Introduction

Carbon-fiber composites may provide high passenger safety owing to excellent energy absorption capabilities in case of collision: energy is dissipated in these materials through multiple failure mechanisms, such as delamination, fiber breakage, and matrix cracking [1-4]. This makes it possible to consider composites in the design of frontal crash rails—automotive parts which are intended to absorb impact energy during collision.

Finite element simulations have been widely used to evaluate and compare the performance of composite energy absorbers, where explicit finite element codes, such as LS-DYNA, have been utilized. These codes offer users a wide range of phenomenological macroscale material models for simulating impacts on composite structures. For example LS-DYNA currently offers more than 25 material models suitable for general impact simulations with composites [5]. It is, therefore, imperative to identify among pre-existing models those that are suitable specifically for crash modeling, understand their limitations and formulate best practices for their use.

Several studies have examined the applicability of pre-existing material models in LS-DYNA. For example, Feraboli et al. [6] investigated the applicability of LS-DYNA's MAT_ENHANCED_COMPOSITE_DAMAGE (MAT054) to modeling of the axial crushing of composite sinusoidal specimens. It was concluded that, although correlation with experimental data could be achieved, the material model did not demonstrate real predictive capabilities and required extensive calibration. MAT054 model was also used by Boria et al. [7] to simulate impact behavior of CFRP frontal impact attenuator under crushing load, and good agreement with the experimental results was reported by the authors. Xiao et al. [8] conducted axial crush simulations of braided carbon tubes using LS-DYNA MAT58 material model. The authors reported 20% overprediction of the peak load and a significant underprediction of both average crush forces and energy absorption levels, as compared with experimental data. Andersson and Liedberg [9] conducted axial crush simulations with MAT262 model using uniform and irregular meshes. It was reported that both cases could be trimmed such that the results correlate well with the test data. McGregor et al. [10-11] investigated the applicability of a continuum damage mechanics-based material model CODAM (implemented in LS-DYNA as MAT219) for modeling of axial crushing of braided composite tubes. The material model uses a sub-laminate rather than a common ply-by-ply representation of composite and, thus, requires non-standard tests for material characterization [12]. It was found to be cable of adequately predicting the failure characteristics and energy absorption of the tubes.

In most of the outlined studies, only a single material model was considered throughout the study and tuned for given impact conditions. The intent of this work is to compare with each other the predictive capabilities of several pre-existing composite material models, when they are used for axial crush simulations. To narrow down the choice when selecting material models for the comparative evaluation, the following criteria were applied. First, only LS-DYNA models formulated in terms of individual ply properties were considered, such that mechanical properties required as input for these models can be fully characterized by standard experiments. Second, the models must be applicable to shell elements, which are the most common choice for vehicle crash simulations in industry. Also, only material models applicable for thermoset matrix continuous fiber composites were studied, which excludes from consideration multiple available models that specific to short- and long-fiber thermoplastics. With these criteria in mind, the following three material models were chosen for further investigations: *MAT_ENHANCED_COMPOSITE_DAMAGE (MAT054), *MAT_LAMINATED_COMPOSITE_FABRIC (MAT058) and *MAT_LAMINATED_FRACTURE_DAIMLER_CAMANHO (MAT262).

2. Material models

As it is common with macroscale material models, MAT054, MAT058 and MAT262 are formulated in terms of both mechanical properties and non-physical parameters, such as, for example, element erosion strains, stress limit factors, etc. For all simulations, mechanical properties of a unidirectional IM7/8552 lamina adopted from the world-wide failure exercise [13] were used. These properties are summarized in Table 1.

Table 1 - Mechanical properties of IM7/8552 composite

Property	Units	Value	Material model
Mass density, RO	kg/mm3	1.58E-06	All three
Young's modulus - longitudinal direction, EA	MPa	165000	All three
Young's modulus - transverse direction, EB	MPa	9000	All three
Poisson's ratio (minor), PRBA / PRCA	–	0.0185	All three
Poisson's ratio cb, PRCB	–	0.5	All three
Shear modulus , GAB / GCA	MPa	5600	All three
Shear modulus BC, GBC	MPa	2800	All three
Fracture toughness for longitudinal (fiber) compressive failure mode, GXC	N/mm	79.9*	MAT262
Fracture toughness for longitudinal (fiber) tensile failure mode, GXT	N/mm	91.6*	MAT262
Fracture toughness for transverse (fiber) compressive failure mode, GYC	N/mm	0.76*	MAT262
Fracture toughness for transverse (fiber) tensile failure mode, GYT	N/mm	0.2**	MAT262
Fracture toughness for in-plane shear failure mode, GSL	N/mm	0.8**	MAT262
Longitudinal compressive strength, XC	MPa	1590	All three
Longitudinal tensile strength, XT	MPa	2560	All three
Transverse compressive strength, YC	MPa	185	All three
Transverse tensile strength, YT	MPa	73	All three
Shear strength, SL	MPa	90	All three
Fracture angle in pure transverse compression, FIO	deg.	53	MAT262
In-plane shear yield stress, SIGY	MPa	60	MAT262
Tangent modulus for in-plane shear plasticity, ETAN	MPa	750	MAT262
Strain at longitudinal compressive strength, E11C	–	0.011	MAT058
Strain at longitudinal tensile strength, E11T	–	0.01551	MAT058

Strain at transverse compressive strength, E22C	–	0.032	MAT058
Strain at transverse tensile strength, E22T	–	0.0081	MAT058
Engineering shear strain at shear strength, GMS	–	0.05	MAT058

* Due to the lack of experimental data specific to IM7/8552, this property was assumed to be the same as measured experimentally in [14] for T300/1034-C composite;
** GYT = G_Ic, and GSL = G_IIc.

MAT_054, or *MAT_ENHANCED_COMPOSITE_DAMAGE, is the most commonly used material model in crash simulations with composites. It assumes ply level linear elastic orthotropic response up to failure, with no pre-peak or post-peak softening. Details of implementation of this and other considered models can be found in [5]. The material model takes into account a decrease of longitudinal compressive strength of a ply (XC) in case of transverse matrix failure, caused by reduction of matrix efficiency in supporting fibers against microbuckling. This is represented by a reduction factor YCFAC, such that the compressive strength in the fiber direction after compressive matrix failure is reduced to $X_C = YCFAC \cdot Y_C$.

As with all other material models, MAT054 has a set of non-physical input parameters, which can be categorized into 3 groups: erosion parameters, parameters controlling crashfront softening, and those characterizing material behavior after failure initiation. All of the non-physical parameters of MAT054, together with the rationale used for their initial choice, are listed in Table 2. A typical stress-strain curve for MAT054 is schematically shown in Fig. 1.

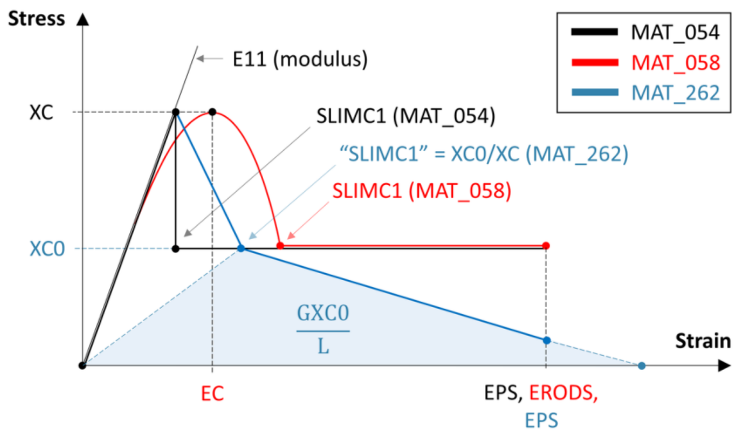

Figure 1 – Comparison of MAT054, MAT058 and MAT262

Table 2 - Non-physical parameters for MAT054 (initial pre-calibration values)

Parameter	Meaning	Units	Value	Comment for the chosen initial value
DFAIL_	Maximum strains for directional strainings at which element will be eroded.	mm/mm		Disabled to control elements' erosion by timestep (TFAIL) and effective strain (EPS) only.
TFAIL	Element is deleted when its time step is smaller than the given value.	s	1E-07	Element is deleted when current timestep is less 1e-7 s.
EPS	Effective failure strain	mm/mm	0.55	Chosen as to be significantly higher than any directional strain at failure initiation.
SOFT	Softening reduction factor for material strength in crashfront elements,	–	0.57	A value suggested in [6], based on calibration with experimental data.
SOFT2	Optional transverse softening reduction factor.	–	no input	Softening is assumed to be isotropic
PFL	Percentage of layers which must fail until crashfront is initiated.	–	100	Default value
BETA	Weighting factor for shear term in tensile fiber mode.	–	0.00	No effect of shear stresses on fiber tensile failure (max stress criterion), which usually provides good agreement with experimental data.
SLIMT1	Factor to determine the minimum stress limit after stress maximum (fiber tension).	–	0.01	Small but non-zero residual strength is assumed after tensile failure to avoid numerical instabilities
SLIMC1	Factor to determine the minimum stress limit after stress maximum (fiber compression).	–	1.00	A recommended value [5]

SLIMT2	Factor to determine the minimum stress limit after stress maximum (matrix tension).	–	0.10	A recommended value [5]
SLIMC2	Factor to determine the minimum stress limit after stress maximum (matrix compression).	–	1.00	A recommended value [5]
SLIMS	Factor to determine the minimum stress limit after stress maximum (shear).	–	1.00	A recommended value [5]
FBRT	Reduction factor for fiber tensile strength after matrix compressive failure.	–	0.00	A zero effect of transverse matrix cracking on fiber tensile strength is assumed.
YCFAC	Reduction factor for compressive fiber strength Xc after matrix compressive failure.	–	2.00	Default value.

MAT058, or *MAT_LAMINATED_COMPOSITE_FABRIC, is a damage mechanics-based model, which accounts for pre- and post-peak softening of composite plies. Both pre- and post-peak softening are assumed to be non-linear in this model. The details of implementation of this model can be found in [15]. Non-physical parameters associated with MAT058, as well as rationale for their choice, are described in Table 3. A typical stress-strain curve for MAT058 is schematically shown in Fig. 1.

Table 3 - Non-physical parameters for MAT058 (initial pre-calibration values)

Parameter	**Meaning**	**Units**	**Value**	**Comment for the chosen initial value**
TSIZE	Time step for automatic element deletion.	s	1E-07	Element is deleted when current timestep is less 1e-7 s.
ERODS	Maximum effective strain for element failure. If lower than zero, element fails when effective strain calculated from the full strain tensor exceeds ERODS	mm/mm	-0.55	Chosen as to be significantly higher than any directional strain at failure initiation.
SOFT	Softening reduction factor for material strength in crashfront elements,	–	0.57	A value suggested in [6], based on calibration with experimental data.
SLIMT1	Factor to determine the minimum stress limit after stress maximum (fiber tension).	–	0.01	Small but non-zero residual strength is assumed after tensile failure to avoid numerical instabilities
SLIMC1	Factor to determine the minimum stress limit after stress maximum (fiber compression).	–	1.00	A recommended value [5]
SLIMT2	Factor to determine the minimum stress limit after stress maximum (matrix tension).	–	0.10	A recommended value [5]
SLIMC2	Factor to determine the minimum stress limit after stress maximum (matrix compression).	–	1.00	A recommended value [5]
SLIMS	Factor to determine the minimum stress limit after stress maximum (shear).	–	1.00	A recommended value [5]

MAT262 is an orthotropic continuum damage model for laminated fiber-reinforced composites. The model assumes bi-linear post-peak softening for the longitudinal direction and linear softening for the transverse direction and shear. Damage activation functions based on the LaRC04 failure criteria [16-17] are used to predict the different failure mechanisms occurring at the ply level.

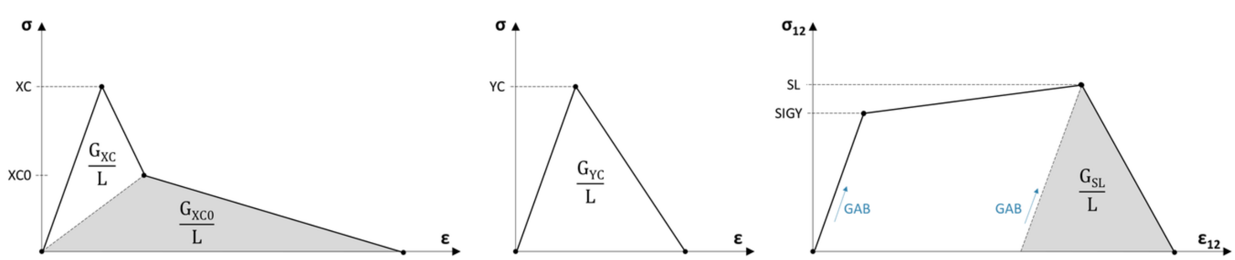

Figure 2 – Stress-strain curves and damage evolution laws for MAT_262

Two damage evolution laws are assumed in MAT262: bi-linear for the longitudinal direction, and linear for the transverse direction and in-plane shear, as shown in Fig. 2. The non-physical parameters of MAT262, as well as rationale for their choice, are described in Table 4.

Table 4 – Non-physical parameters for MAT262 (initial pre-calibration values)

Parameter	Meaning	Units	Value	Comment for the chosen initial value
D__F	Flag to control failure of an integration point (DAF - longitudinal tensile failure; DKF - longitudinal compressive failure; DMF - transverse failure): EQ.0.0: IP fails if any damage variable reaches 1.0; EQ.1.0: no IP failure	–	1	Disabled to control elements' erosion by effective strain (EPS) only.
EPS	Maximum effective strain for element layer failure. GT.0.0: effective strain calculated assuming material is volume preserving; LT.0.0: effective stress calculated from the full strain tensor.	mm/mm	-0.55	Chosen as to be significantly higher than any directional strain at failure initiation.
SOFT	Softening reduction factor for material strength in crashfront elements	–	0.57	A value suggested in [6], based on calibration with experimental data.
PFL	Percentage of layers which must fail until crashfront is initiated.	–	100	Default value
GXCO	Fracture toughness for longitudinal (fiber) compressive failure mode to define bi-linear damage evolution.	N/mm	1526	Calculated as GXCO = f(XCO, L, ϵ_{fr}), see below.
GXTO	Fracture toughness for longitudinal (fiber) tensile failure mode to define bi-linear damage evolution.	N/mm	30.7	Calculated as GXTO = f(XTO, L, ϵ_{fr}), see below.
XCO	Longitudinal compressive strength at inflection point.	MPa	1272	Assuming that XCO = 0.8 x XC
XTO	Longitudinal tensile strength at inflection point.	MPa	25.6	Assuming that XTO = 0.01 x XT

Several important notes must be made with regards to implementation of fracture toughness in this model. First, the model uses a common approach of normalizing the fracture toughness by a characteristic length of the element, in order to ensure that the energy needed to withstand the crack is the same regardless of the element size. However, if the element size is set too large, "snapback" can occur, resulting in a failed simulation [9]. Snapback occurs when the strain is forced to be reduced even though the element is supposed to be elongated due to the loading. To avoid this, there exists a critical element size, which is defined in the model as a function of the actual fracture toughness, strength and Young's modulus of the material:

$$l_{elem} \leq \frac{2E_M \cdot G_M}{X_M^2}, \quad (1)$$

where M = 1+, 1-, 2+, 2-, 6.

If element is not small enough to satisfy this condition, the fracture toughness will be automatically adjusted by the solver. For example, with the material properties as defined in Table 1, the element size in simulation must not be larger than 0.68 mm, which is normally an impractically small value for the full-scale crash simulations. On the other hand, if 4 mm elements will be used, the solver will use the value of GYT of about 6 times higher as compared with the physically-based value presented in Table 1. Correspondingly, "fracture toughness" in this model should be considered as another artificial parameter, which controls post-failure behavior of composite, rather than a physical property.

Second, the stress-strain behavior in the fiber direction is bi-linear after failure for both compression and tension. The ratios $\frac{XCO}{XC}$ and $\frac{XTO}{XT}$ can be viewed as being similar to the stress limit factors (SLIMC_) of MAT054 and MAT058 (see Fig. 1). However, this implementation provides more flexibility, as the stress may decrease gradually rather than necessarily remain at the same level. This behavior is controlled by parameters GXCO and GXTO. It can be deduced from Fig. 1 that, for example, GXCO can be expressed as a function of strength at inflection point (XCO), characteristic element length (L) and some "fracture strain" (ϵ_{fr}), at which the stress-strain curve intersects the horizontal axis:

$$GXCO = \frac{L}{2} \cdot XCO \cdot \epsilon_{fr} \quad (2)$$

To ensure that element has some resistance to stress in longitudinal direction up until erosion, the value of fracture strain in the expression above must be such that $\epsilon_{fr} \geq EPS$, where EPS is erosion strain. In this study, GXCO and GXTO were calculated assuming $\epsilon_{fr} = 0.60$, whereas erosion strain of 0.55 was used in all simulations. The initial values of GXCO and GXTO represented in Table 4, were determined assuming that $\frac{XCO}{XC} = 0.8$ (by analogy with large SLIMC1 used with MAT054/058) and $\frac{XTO}{XT} = 0.01$ (same as SLIMT1 = 0.01 used with MAT054/058).

3. Experimental Data

In this study, experimental results from the Oak Ridge National Laboratory (ORNL) composites crush test database [18] were used to access and compare predictive capabilities of MAT054, MAT058 and MAT262 in crash simulations. In particular, tests No. 46B and 47B from the database were chosen for initial evaluation of the models. Both axial crush tests were performed at Oak Ridge National Laboratory at the same conditions and with the same configuration of the energy absorbers - square cross-section IM7/8552 CFRP tubes with quasi-isotropic layup ($[0_2/\pm45_2/90_2]_s$) and 0.135 mm ply thickness, rounded corners and bevel-shaped crush initiators. Composite tubes for the tests were manufactured at the University of Utah [19]. With this particular layup and geometry, the specimens exhibited so-called brittle failure mode, which is, as opposed to fiber splaying, characterized by relatively low energy absorbed through friction and delamination.

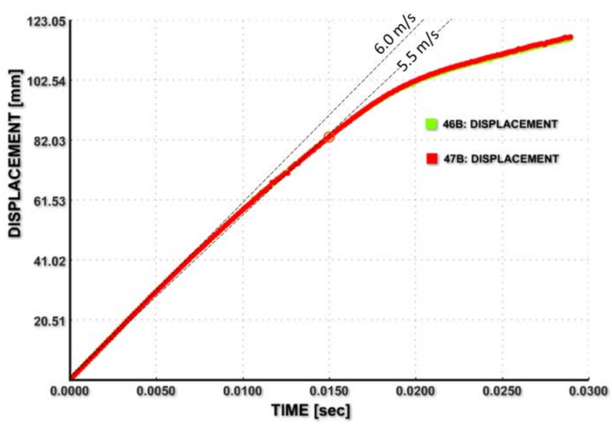

Figure 3 – Crosshead speed in the impact experiments

Tests were conducted using a 500 kN servo-hydraulic test machine [20] at the constant speed of 5.5 m/s. The machine's crosshead displacement-time diagrams for the tests are shown in Fig. 3. It can be seen in the figure that the constant speed of crushing was maintained in the tests only up until time of 15 ms after initiation. From that moment, recorded speed of crosshead changes non-linearly. Correspondingly, all simulations presented in this study were conducted with a constant speed of loading equal to 5.5 m/s, and with the termination time set to 15 ms. Total energy absorbed by the tubes within the first 15 ms after initiation of crushing was calculated to be equal to 3020 J (mean value for experiments 46B and 47 B; standard deviation - 9 J). Energy absorbed in the "stable crushing regime", which approximately starts 2 ms after crushing initiation (crosshead moves 11 mm by that time), equals to 2678 J (mean value for 46 B and 47 B; standard deviation - 26 J).

4. Numerical Model

A numerical model developed to represent the ORNL crush tests No. 46B and 47B is shown in Fig. 4. This is a single shell layer model with shell elements of approximately 3.5 mm in size used for discretization. It should be noted that a mesh sensitivity study conducted in [7] with a crush tube of similar dimensions as the one considered in this study and the same element type, found meshes up to 5 mm being fully satisfactory for the given type of analysis. LS-DYNA's default element formulation ELFORM = 2 with Reissner-Midlin kinematics (straight and unstretched cross-sections; shear deformations possible) was used with all shell elements in this study. The laminated shell theory was invoked for all composite elements to account for non-uniform trough-the-thickness shear strain by setting the parameter LAMSHT = 1 (or LAMSHT = 3 for MAT262) in the *CONTROL_SHELL card.

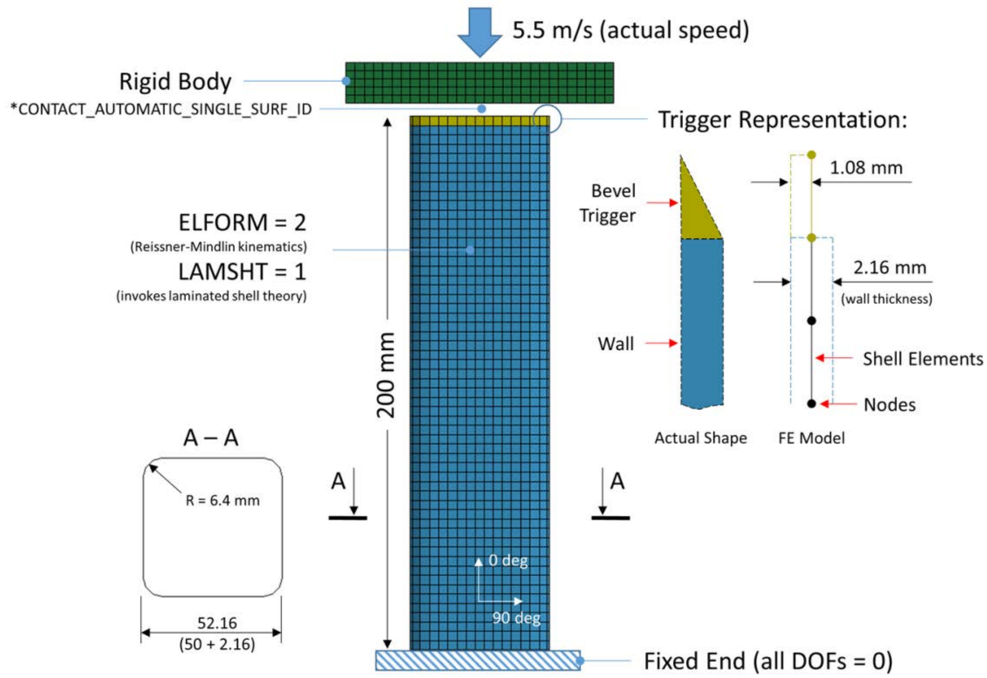

Figure 4 – LS-DYNA model for axial crush simulations

The model consists of three parts, representing, correspondingly, the tubular test specimen, bevel-shaped crush trigger and the loading plate. The loading plate was represented as a rigid body in the model. Elements representing the part of the tube with the regular cross-section were assigned the quasi-isotropic $[0_2/\pm45_2/90_2]_s$ layup with a ply thickness of 0.135 mm and the total thickness of 2.16 mm. The bevel-shaped trigger was represented as a single row of elements, which have only half of the layers as compared with the regular-zone layup. The layers in the trigger elements were shifted inwards with respect to the elements' middle surface by specifying a midsurface offset in LS-DYNA. This rather simplified representation of bevel-shaped triggers helped avoiding using small elements and, correspondingly, maintaining reasonably large timesteps in simulations.

The tubes used in physical experiments had slightly conical shape, as mandrels used in their manufacturing were tapered 0.25° to facilitate easy removal of the tubes [19]. This feature of the tubes' geometry was explicitly represented in the numerical model. LS-DYNA's *CONTACT_AUTOMATIC_SINGLE_SURF_ID card [21] was used with the constant friction coefficient of 0.2 to define the contact between the tube and plate, as well as possible self-contact of the tube material. Trigger elements were connected with the rest of the tube through shared nodes.

5. Numerical results

5.1 Axial crush with MAT054

The force-displacement diagram obtained from the simulation with the initial set of MAT054 parameters, as defined in Table 1 and Table 2, is shown by the yellow line in Fig. 5 along with the experimental data. It should be noted that it is common practice during post-processing to filter the numerical results using a low-pass digital filter (SAE) [6]. However, to avoid altering the results, only very high frequency oscillations, exceeding 1000Hz, were filtered in this study. The following main features of the numerical result can be noticed:

1. There exists initial small force peak, also visible in both experimentally obtained curves. This peak corresponds to crushing of the trigger.

2. Predicted large force peak, preceding initiation of stable crushing, is significantly higher than the max force observed in the experiments (approx. 180 kN vs. 70 kN).

3. In the stable crushing regime, predicted average crush force is similar to the crush force observed in both experiments. However, amplitudes of local force peaks in this regime are substantially higher as compared to those on the experimental curves.

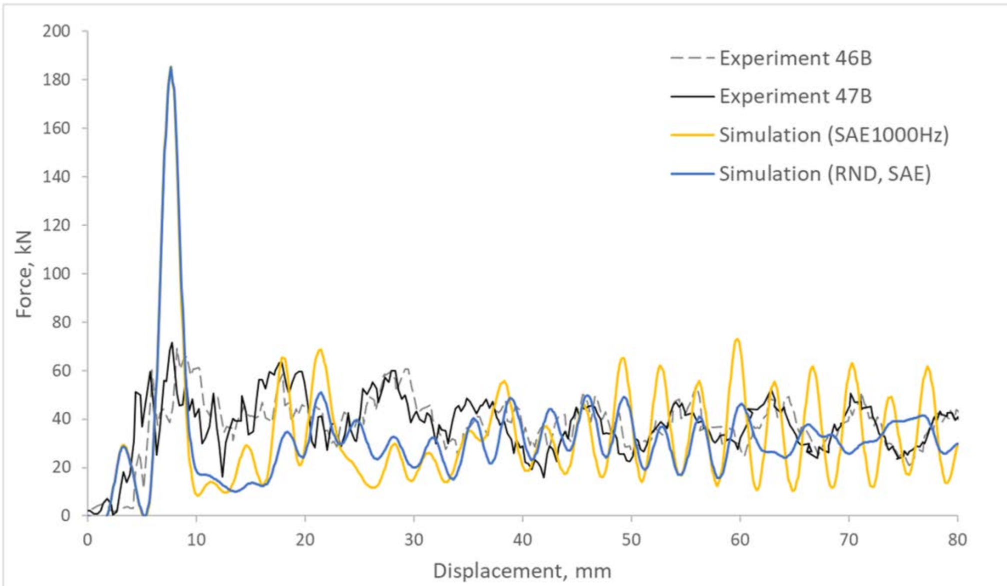

Figure 5 – Force-displacement curves: simulations with MAT054, non-calibrated parameters

To increase the realism of the modeling, the tube model was further modified by representing initial imperfections, such as possible small local deflections of the tube walls from ideally straight shape, which are often induced in manufacturing. This was implemented through randomizing out-of-plane coordinates (ζ_i) of all nodes of the composite tube, such that new out-of-plane nodal coordinates $\zeta_i^{new} = \zeta_i + \Delta$, where Δ is a random number between 0 to 5% of the tube wall thickness, i.e. $\Delta = \pm rnd(0 \ldots\ 0.05 \cdot t_{wall})$. Thus, with the composite tube thickness of 2.16 mm (see Section 4), the out-of-plane position of an individual node can be shifted by a value ranging from 0 to 108 microns.

The effect of such randomization can be observed in Fig. 5 (the blue curve). Although it does not change the value of the predicted peak force or the average crush force, it significantly reduces amplitudes of local force peaks in the stable crushing regime. With the mesh randomization in place, these predicted local force peaks have the amplitudes similar to those observed experimentally. Considering this positive effect of randomization on predictive capabilities of numerical model, all results reported herein obtained with the randomized meshes.

The value for the force peak was found, through the trial and error, being dependent on the stress limit factor in longitudinal compression, SLIMC1. Results of simulations with different values of this parameter are shown in Fig. 6. It can be seen that the force peak reduces with reduction of SLIMC1 parameter. The "optimal" value of SLIMC1, which provides the closest correlation with experimental data, lies between 0.25 and 0.50, as can be deduced from Fig. 6. It was chosen for further simulations as the average of these two boundary values, such as SLIMC1 = 0.375.

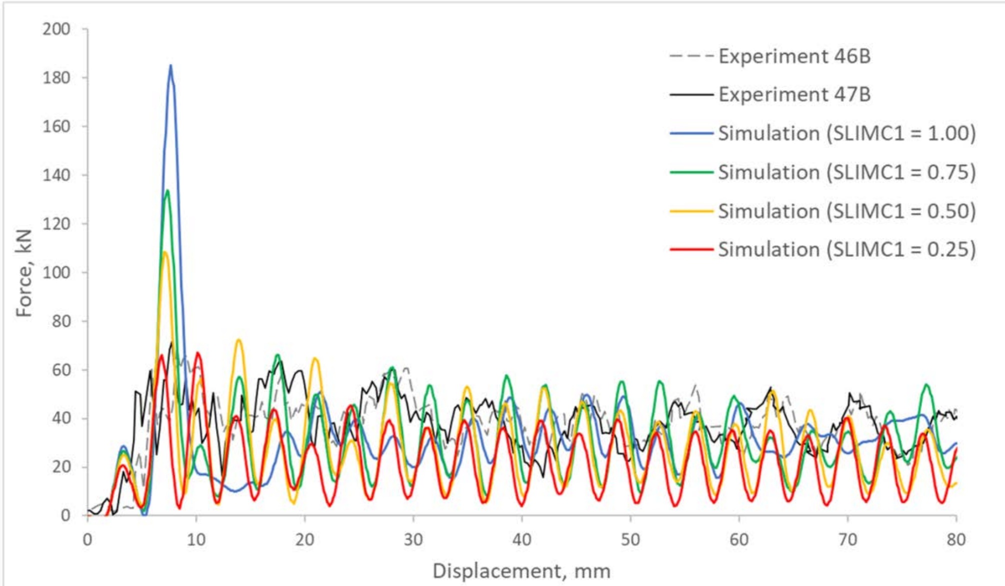

Figure 6 – Force-displacement curves: simulations with MAT054, influence of SLIMC1

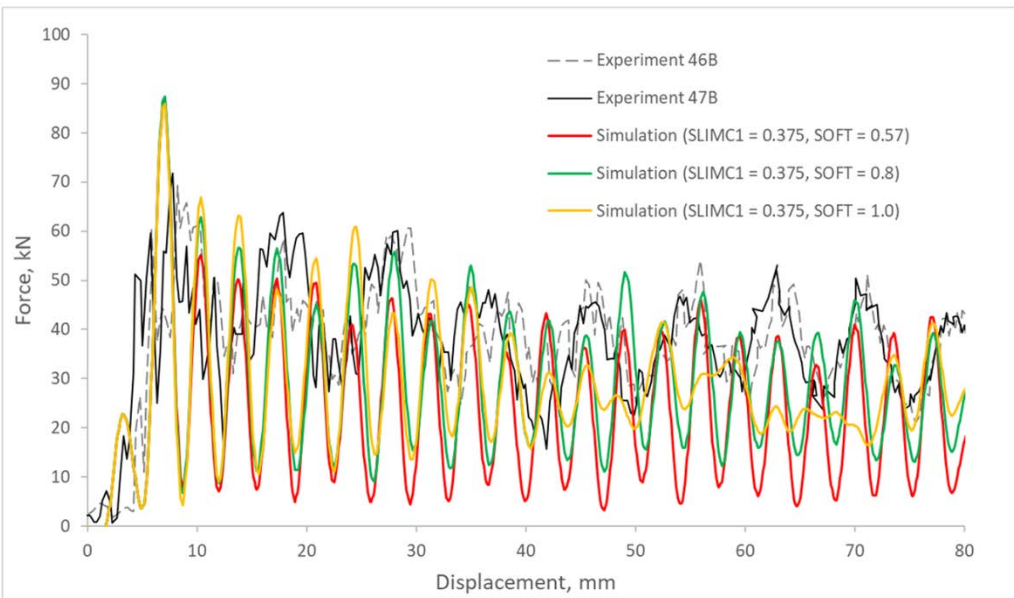

Figure 7 – Force-displacement curves: simulations with MAT054, calibrated parameters

It should be noted, however, that reduction of the stress limit factor from 1.00 to 0.375, also reduced the predicted average crush force. This was addressed by the change of the softening factor SOFT from the initially set value of 0.57 (see Table 2) to higher values. Simulations with different values of this parameter are shown in Fig. 7. It can be seen in the figure that SOFT = 0.8 provides the most reasonable correlation with the experimental data in terms of the average force in the stable crushing regime.

Deformations of the composite tube during crushing are shown in Fig. 8. As can be seen in the figure, with the initial set of parameters simulation predicts local buckling and noticeable out-of-plane deformations of the tube ahead of the crashfront (marked with red arrows in Fig. 8). Such deformations were not observed experimentally. With the calibrated set of parameters (SLIMC1 = 0.375, SOFT = 0.8), the simulation predicts more stable crushing without buckling. Qualitatively, this behavior better represents deformation patterns of the tubes in the experiments 46B and 47B. In terms of energy absorption during stable crushing, simulation with the "default" parameters predicts absorption of 2000 J, while simulation with calibrated parameters predicts 2091 J.

This is, correspondingly, 25% and 22% lower than the energy absorbed by the tubes in experiments (2678 J; see Section 3).

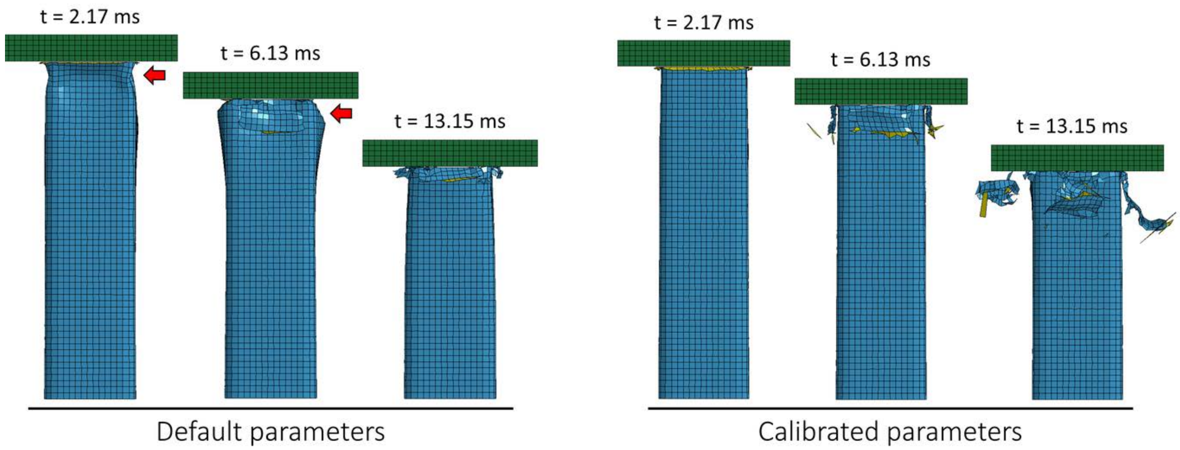

Figure 8 – Deformation of the CFRP tube during axial crushing (simulations)

5.2 Axial crush with MAT058

A similar strategy of calibrating non-physical parameters was employed for MAT058. Figure 9 shows force-displacement diagrams from simulations with different longitudinal compression stress limit factors. As can be seen in the figure, both initially set value of SLIMC1 = 1.0 and the value obtained through calibration for MAT054 (SLIMC1 = 0.375), significantly overpredict the peak force, when used with MAT058. Simulations with further reduced values of this parameter, still result in significant (up to 40%) overprediction. Also, no significant sensitivity of the result (in terms of peak load and crush force) was observed to variations of softening factor in the range of SOFT = 0.5 – 0.9. Such behavior - i.e. peak force overprediction - is believed to be a consequence of inability of MAT058 to account for reduction of longitudinal compressive strength in the case of transverse compressive failure.

To illustrate this behavior, single-element simulations were conducted with a $[0_2/\pm45_2/90_2]_s$ quasi-isotropic laminate loaded in compression. The results of these simulations are shown in the left plot of Fig. 10. Failure of the 90 and ±45 plies is represented by change of slope of the corresponding stress-strain curves. Upon satisfaction of the failure criterion in all plies, laminates' load-carrying capacity does not drop to zero, as stress limit factors SLIMC1 = 1 were used for MAT054 and MAT058, and $XCO = 0.8 \cdot XC$ with large value for GXO parameter were used for MAT262, as discussed in the previous section. MAT058 in this test predicts significantly higher load-carrying capacity of the compression-loaded quasi-isotropic laminate, as compared with the other material models. This results from inability of MAT058 to account for reduction of XC in the case of transverse compressive failure. In fact, if MAT054 would be used with $YFAC = \frac{XC}{YC}$, which is equivalent to the lack of relationship between the matrix failure and longitudinal compressive strength, the simulation would lead to the same prediction as obtained with MAT058. For clarity, this scenario ($YFAC = \frac{XC}{YC} = 8.59$ for MAT054) is shown with dotted line on the right plot in Fig. 10.

Despite of poor prediction of peak force, simulations with MAT058 can be reasonably accurate in predicting average crush force in the stable crushing regime. In this regard, as can be deduced from Fig. 9, most accurate results were obtained with SLIMC1 = 0.375, i.e. the same value as used with MAT054. The predicted energy absorption (stable crushing regime) in the latter case was equal to 2142 J, which is 20% lower than the experimental value.

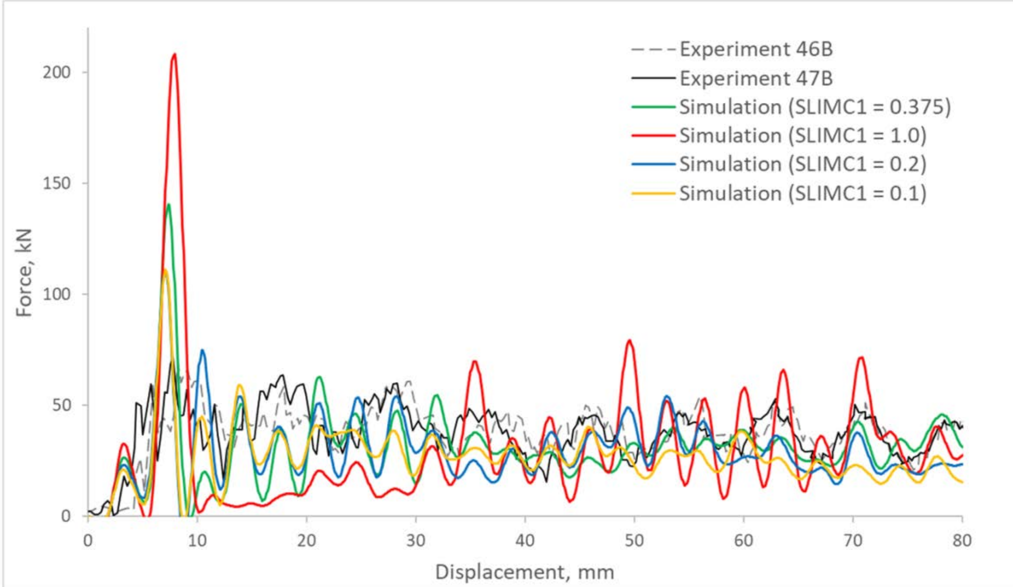

Figure 9 – Force-displacement curves: simulations with MAT058, influence of SLIMC1

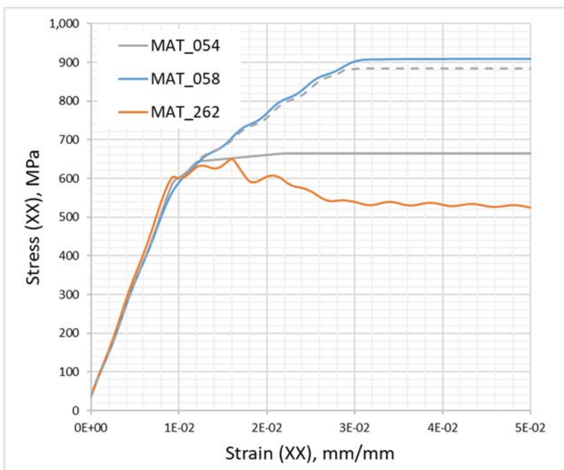

Figure 10 – Single-element compression test with quasi-isotropic layup (right)

5.3 Axial crush with MAT262

Results of simulations (force-displacement plots) for MAT262 with the initial set of parameters, as well as with additional values of stress limit in longitudinal compression are shown in Fig. 11. It should be noted that SLIMC1 in this figure refers to the ratio of longitudinal compressive strength at inflection point (XCO) and the longitudinal compressive strength (XC), rather than to an actual input parameter of MAT262.

A common feature of all simulations presented in Fig. 11 is a significant underprediction of the crush force and, correspondingly, underestimation of energy absorption. Such a response can be at explained by the fact that damaged ply stiffness cumulatively depends on both tensile and compressive damage variables. Hence, if the default values of GXTO and XTO are too low, this will also reduce element's ability to resist compressive loading. It should be noted, however, that there is no physics-based rationale to define these parameters. It, therefore, can be concluded that a simple trial and error approach used for fine-tuning of MAT054 and MAT058, cannot be successfully employed for calibration of MAT262.

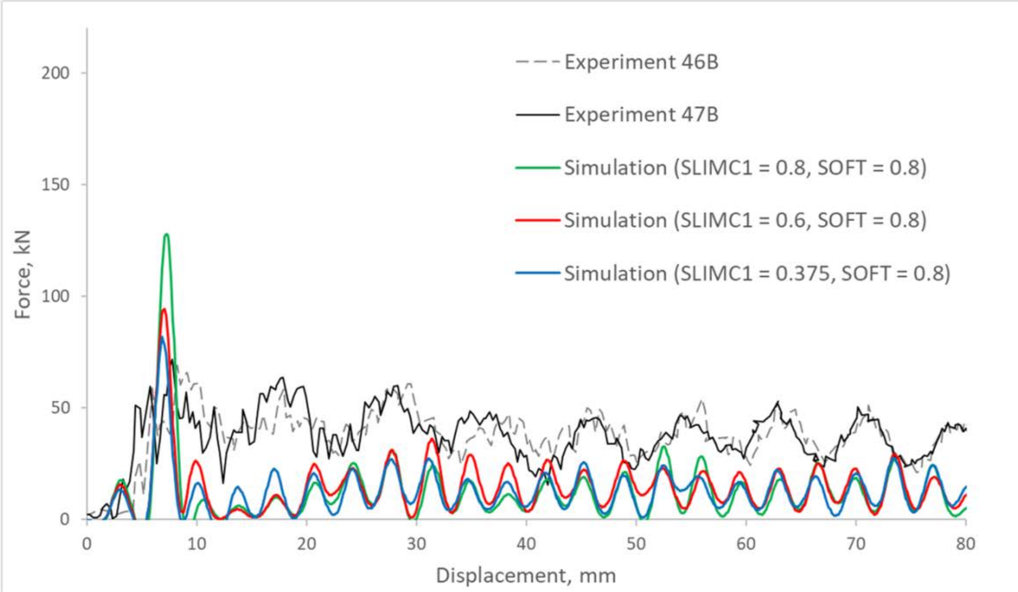

Figure 11 – Force-displacement curves: simulations with MAT262, non-calibrated parameters

In this study, a more formal calibration technique was used for axial crush simulations based on generating a response surface for crush force as a function of MAT262 parameters, which did not have exact physical means for identification. These parameters included longitudinal tensile and compressive strengths at inflection points (XTO and XCO), and fracture angle in pure transverse compression (FIO). For convenience, the former parameters were represented in the form of stress limit factors SLIMT1 and SLIMC1, i.e. as fractions of the corresponding strengths of composite in longitudinal direction. Considering tensile strength at inflection point as a calibration parameter was important, as directional damage coefficients of MAT262 are dependent on contributions to the damage state from both tension and compression. It should also be noted that parameters GXCO and GXTO are dependent properties, which can be calculated as functions of XCO and XTO, and, therefore, were not used for response surface approximation of crush force.

The response surface for crush force as a function of SLIMC1, SLIMT1 and FIO was produced by 1) generating sampling points (i.e. different combinations of SLIMs and FIO) using "Design of experiments" (DOE) approach; 2) evaluating generated sampling points for crush force value using LS-DYNA; and 3) performing regression analysis to obtain response surfaces from sampling point evaluations. For sampling points generation, a face-centered central composite design DOE plan was used [22]. With 3 input parameters, this plan generates the total of 15 sampling points. Stress limits were sampled from the range of SLIM = 0.1 - 0.9. Fracture angle, FIO, was allowed to vary from 45°, which corresponds to fracture along the plane of the maximum shear stress, to 55°, which is the upper bound for fracture angle, observed experimentally in technical composites [16].

Upon evaluation of all sampling points, a response surface for crush force was built using the Genetic Aggregation algorithm, available in ANSYS DesignXplorer [22]. As can be seen in Fig. 12, crush load has a distinctive maximum at some non-trivial combination of SLIMC1 and SLIMT1. At the same time, crush load increases linearly with increase of fracture angle.

As simulations with initial parameters significantly underestimated the crush force, the obtained response surface was used to find a set of non-physical parameters (SLIMC1, SLIMT1 and FIO) that provides the maximum possible crush force. This maximum was located on the response surface using a Nonlinear Programming by Quadratic Lagrangian method [22], which represents a gradient-based optimization technique. The corresponding values of the non-physical parameters were as follows: SLIMC1 = 0.86, SLIMT1 = 0.83 and

FIO = 55. A force-displacement curve, corresponding to a simulation with these parameters, is shown in Fig. 13 as a blue line. The curve reasonably well correlates with the experimental data in the stable crushing regime.

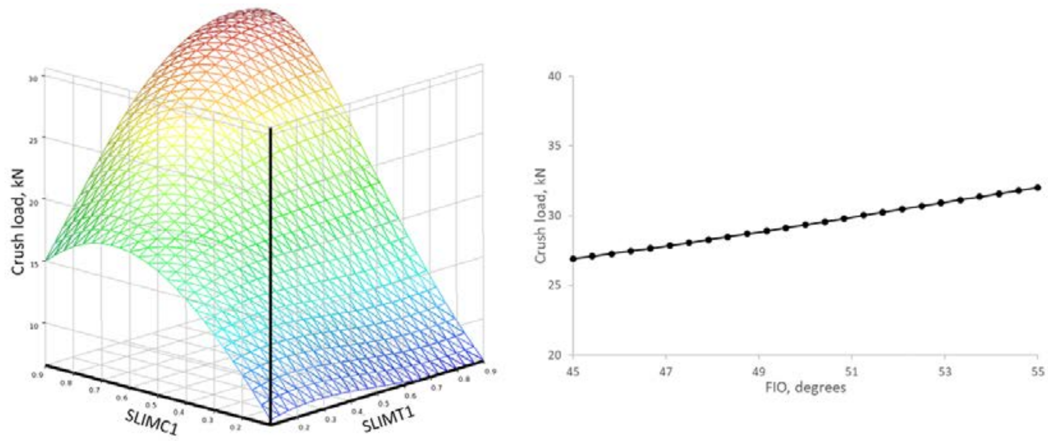

Figure 12 – Response surface approximation of crush force as a function of MAT262 non-physical parameters

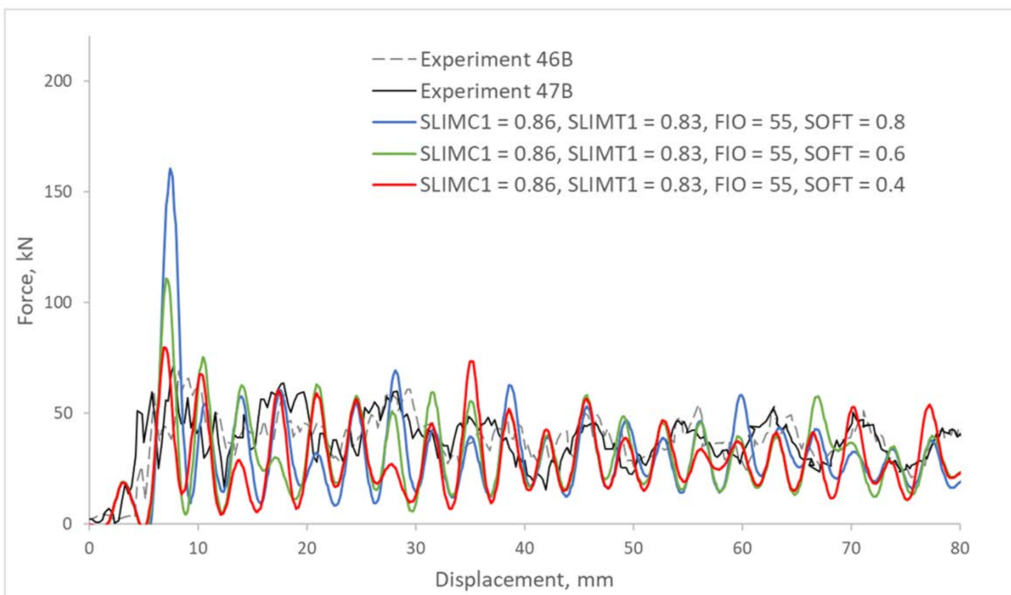

Figure 13 –Force-displacement curves: simulations with MAT262, calibrated parameters

With MAT262, softening factor (SOFT) was found to be a parameter mainly affecting the value of the peak load and having no significant influence on crush force during stable crushing. Therefore, it was kept constant (SOFT = 0.8) in parameter calibration for crush force, and was adjusted separately. It can be seen in Fig. 13, that SOFT = 0.4 results in prediction of the peak force that reasonably well correlates with the experimental data. In terms of energy absorption in stable crushing, MAT262 with SLIMC1 = 0.86, SLIMT1 = 0.83, FIO = 55 and SOFT = 0.4, predict absorption of 2015 J within the first 15 ms, which is only 25 % lower than the experimental value.

5.4 Use of Calibrated Models in Simulations with a Different Layup

Now with the three material model parameter sets calibrated for one particular layup, these were used in similar simulations with a distinct layup. This represents a common practice in industry when only a single set of experimental data is available to test and tune the numerical models, and further design is conducted with the "as-calibrated" parameters. It is, therefore, imperative to understand predictive capabilities of such models when different layups are considered in the design process.

The following configurations of fiber angles was considered: $[(90_2/\pm60)_2]_s$. This layup correspond to the one used in the tests No. 50F - 51F, conducted at the Oak Ridge National Laboratory [18]. Except differences in fiber orientation angles, the other conditions of the tests No. 50F - 51F, including the impact speed and composite tubes geometry, were identical to those used in the tests No. 47B - 47B with the quasi-isotropic layup as described in Section 3.

With the $[(90_2/\pm60)_2]_s$ layup, total energy absorbed by the tubes within the first 15 ms after initiation of crushing was experimentally found to be equal to 2358 J (mean value for experiments 50F and 51F; standard deviation - 17 J). In stable crushing, tubes with this layup absorb 2073 J (mean value for experiments 50F and 51F; standard deviation - 13 J). Results of simulations representing these experiments are shown in Fig. 14.

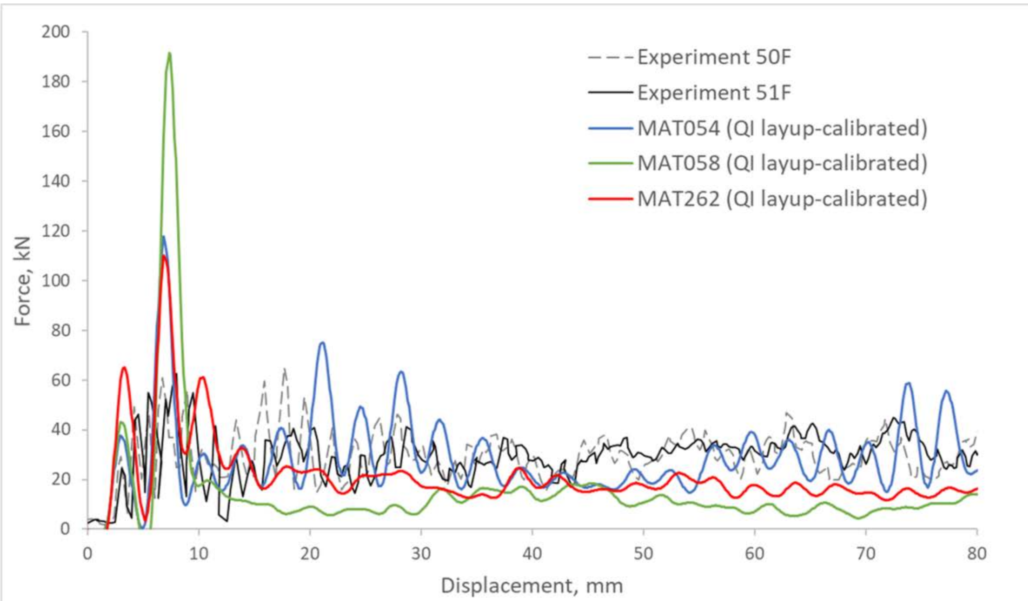

Figure 14 – Force-displacement curves: [(902/±60)2]s layup

All three models overpredict the initial peak force. MAT054 and MAT262 yield to approximately the same value of the peak force, almost twice overpredicting the experimental value. With MAT058, the peak force is overpredicted by a factor of 3. As described in the previous sections, large overprediction of peak force was feature common to all simulations with MAT058.

In the stable crushing regime, simulation with MAT054 results in a reasonably accurate prediction of the crush load. Energy absorbed in stable crushing in this case equals to 1997 J, which is only 4% lower than in the experiment. In contrast, simulation with MAT058 resulted in a very low prediction of energy absorption during crushing (approx. 50% lower than in experiments). It should be noted that this simulation also results in an improper prediction of the mode of failure, as depicted in Fig. 15. Instead of stable crushing observed experimentally, simulation with MAT058 and "as-calibrated" parameters predicts global buckling of the tube, which then loses its ability to resist crushing load efficiently. This can be attributed to the overestimation of load-carrying capacity of the compression-loaded laminates by MAT058, as was discussed earlier in this paper. In case of crush simulations, this can promote other failure modes, such as global buckling, ahead of the local crushing. With MAT262, simulation somewhat underestimated the crush load and predicted absorption of 1266 J during stable crushing. This is 28% lower as compared with experimental data.

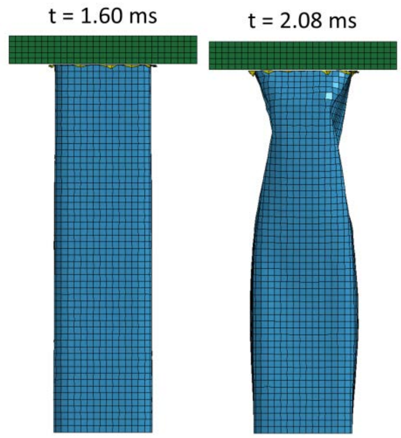

Figure 15 – A non-physical failure mode (global buckling) observed in simulation with MAT058 for $[(90_2/\pm60)_2]_s$ layup

6. Conclusions

In this study, predictive capabilities of three LS-DYNA composite material models – MAT054, MAT058 and MAT262 – were investigated and compared with respect to modeling of axial crushing of CFRP energy absorbers. The three material models were described together with the initial sets of non-calibrated model-specific input data. Results of crush simulations with non-calibrated material models were compared with available experimental data, and then parameter tuning was conducted to improve correlation with experiments. Furthermore, calibrated material models were used in crash simulations with a composite layup that is different from the one employed in calibration.

The following conclusions can be made with regard to applicability of the considered material models to axial crush simulations:

- All three considered material models require extensive calibration to achieve correlation with experimental data. Without calibration, using default or recommended values for non-physical parameters can result in erroneous representation of composite crushing. This is especially the case for MAT262, which demonstrated high discrepancy between simulation and experiment in terms of peak load, crush load and energy absorption, when initial, i.e. not calibrated, set of parameters was used.
- For MAT054 and MAT058, most influencing non-physical parameters that require calibration in axial crush simulations are the stress limit factor in longitudinal compression (SLIMC1) and the crashfront softening factor (SOFT). As only two parameters can be varied, calibration of these two material models can be conducted using a simple trial and error approach. An important factor, limiting the use of MAT058 in axial crush simulations is its inability to account for reduction of longitudinal compressive strength in the case of transverse compressive failure. This was found to consistently result in overestimation of the peak load in simulations with MAT058, and also resulted in prediction of non-physical failure modes. Lacking such a limitation, MAT054 was found in most of considered cases to be able to provide reasonable agreement with experimental data.
- For MAT262, the following parameters were found to be influencing and, thus, requiring calibration: XCO, XTO, FIO, SOFT, GXCO, GXTO. Number of calibration parameters can be reduced by assuming relationships between GXCO, GXTO and corresponding strengths at inflection points (XCO, XTO), as described in Section 2.. However, even in this case calibration would require significant efforts and use of

such techniques, as response surface approximation and optimization. Upon calibration, simulations with MAT262 can in many cases quite well agree with experimental data.

- As results of simulations with the considered models are sensitive and significantly dependent on a proper choice of multiple model-specific damage parameters, it would be beneficial in the future studies to develop a robust first principles-based material model, which would minimize the number of unknown parameters requiring calibration.

With regard to modeling approach for crash simulations, randomization of out-of-plane nodal coordinates was found to be useful as a mean of increasing realism of the models and obtaining better correlation with experimental data. Even small perturbations of nodal coordinates (within 100 microns) enabled more physical representation of local force peaks in the stable crushing regime. Accounting for other forms of manufacturing-induced defects, such as fiber misalignments or undulations, may also contribute to improving the simulations.

Acknowledgements

The authors would like to thank the Natural Sciences and Engineering Research Council of Canada (NSERC) for financial support through Collaborative Research and Development Grant No. CRDPJ 507776 – 16, as well as sponsors from Honda R&D Americas, Hexion Inc., Zoltek Corp. and LAVAL International.

References

1. Lu, Guoxing, and Tongxi Yu. 2003. “Composite Materials and Structures”. In *Energy Absorption of Structures and Materials*, 317–50. Elsevier. doi:10.1533/9781855738584.317.

2. Mamalis, A.G, M. Robinson, D.E. Manolakos, G.A. Demosthenous, M.B. Ioannidis, and J. Carruthers. 1997. “Crashworthy Capability of Composite Material Structures”. *Composite Structures* 37 (2). Elsevier BV: 109–34. doi:10.1016/s0263-8223(97)80005-0.

3. Mamalis, A.G., D.E. Manolakos, M.B. Ioannidis, and D.P. Papapostolou. 2005. “On the Crushing Response of Composite Sandwich Panels Subjected to Edgewise Compression: Experimental”. *Composite Structures* 71 (2). Elsevier BV: 246–57. doi:10.1016/j.compstruct.2004.10.006.

4. Hwang, W-C, C-S Cha, and I-Y Yang. 2011. “Optimal Crashworthiness Design of CFRP Hat Shaped Section Member under Axial Impact”. *Materials Research Innovations* 15 (sup1). Informa UK Limited: s324–s327. doi:10.1179/143307511x12858957674472.

5. LS-DYNA KEYWORD USER’S MANUAL VOLUME II: Material Models, LIVERMORE SOFTWARE TECHNOLOGY CORPORATION (LSTC), 2013.

6. Feraboli, Paolo, Bonnie Wade, Francesco Deleo, Mostafa Rassaian, Mark Higgins, and Alan Byar. 2011. “LS-DYNA MAT54 Modeling of the Axial Crushing of a Composite Tape Sinusoidal Specimen”. *Composites Part A: Applied Science and Manufacturing* 42 (11). Elsevier BV: 1809–25. doi:10.1016/j.compositesa.2011.08.004.

7. Boria, S., J. Obradovic, and G. Belingardi. 2015. “Experimental and Numerical Investigations of the Impact Behaviour of Composite Frontal Crash Structures”. Composites Part B: Engineering 79 (September). Elsevier BV: 20–27. doi:10.1016/j.compositesb.2015.04.016.

8. Xiao, Xinran, Mark E. Botkin, and Nancy L. Johnson. 2009. “Axial Crush Simulation of Braided Carbon Tubes Using MAT58 in LS-DYNA”. Thin-Walled Structures 47 (6-7). Elsevier BV: 740–49. doi:10.1016/j.tws.2008.12.004.

9. M. Anderssen, P. Liedberg. 2014. “Crash Behavior of Composite Structures. A CAE Benchmarking Study.”. Master’s thesis, http://publications.lib.chalmers.se/records/fulltext/199981/199981.pdfhttp://publications.lib.chalmers.se/records/fulltext/199981/199981.pdf - page=50.

10. McGregor, Carla, Reza Vaziri, and Xinran Xiao. 2010. "Finite Element Modelling of the Progressive Crushing of Braided Composite Tubes under Axial Impact". *International Journal of Impact Engineering* 37 (6). Elsevier BV: 662–72. doi:10.1016/j.ijimpeng.2009.09.005.

11. McGregor, Carla, Navid Zobeiry, Reza Vaziri, Anoush Poursartip, and Xinran Xiao. 2017. "Calibration and Validation of a Continuum Damage Mechanics Model in Aid of Axial Crush Simulation of Braided Composite Tubes". *Composites Part A: Applied Science and Manufacturing* 95 (April). Elsevier BV: 208–19. doi:10.1016/j.compositesa.2017.01.012.

12. Zobeiry, N., A. Forghani, C. McGregor, S. McClennan, R. Vaziri, and A. Poursartip. 2017. "Effective Calibration and Validation of a Nonlocal Continuum Damage Model for Laminated Composites". *Composite Structures* 173 (August). Elsevier BV: 188–95. doi:10.1016/j.compstruct.2017.04.019.

13. Kaddour, AS, MJ Hinton, PA Smith, and S Li. 2013. "Mechanical Properties and Details of Composite Laminates for the Test Cases Used in the Third World-Wide Failure Exercise". *Journal of Composite Materials* 47 (20-21). SAGE Publications: 2427–42. doi:10.1177/0021998313499477.

14. Pinho, S. T. 2005. "Modelling Failure of Laminated Composites Using Physically-Based Failure Models". PhD thesis, University of London.

15. Matzenmiller, A., J. Lubliner, and R.L. Taylor. 1995. "A Constitutive Model for Anisotropic Damage in Fiber-Composites". *Mechanics of Materials* 20 (2). Elsevier BV: 125–52. doi:10.1016/0167-6636(94)00053-0.

16. Davila C.G. Pinho S.T.. Failure Models and Criteria for FRP Under In-Plane or Three-Dimensional Stress States Including Shear Non-Linearity. NASA/TM-2005-213530, 2005. https://ntrs.nasa.gov/archive/nasa/casi.ntrs.nasa.gov/20050110223.pdf.

17. Maimí, P., P.P. Camanho, J.A. Mayugo, and C.G. Dávila. 2007. "A Continuum Damage Model for Composite Laminates: Part I Constitutive Model". *Mechanics of Materials* 39 (10). Elsevier BV: 897–908. doi:10.1016/j.mechmat.2007.03.005.

18. Crashworthiness of Carbon Fiber Composites. http://energy.ornl.gov/CFCrush/rate_tests/rate_tests.cgi.

19. Courteau, M.A. 2011. "INVESTIGATING THE CRASHWORTHINESS CHARACTERISTICS OF CARBON FIBER/EPOXY TUBES". Master's thesis, University of Utah. http://thyme.ornl.gov/CFCrush/test_method/uou/Courteau_2011.pdf

20. Boeman, Raymond G., and Ari G. Caliskan. 2002. "A Novel Capability for Crush Testing Crash Energy Management Structures at Intermediate Rates". In *SAE Technical Paper Series*. SAE International. doi:10.4271/2002-01-1954.

21. LS-DYNA KEYWORD USER'S MANUAL VOLUME I, LIVERMORE SOFTWARE TECHNOLOGY CORPORATION (LSTC), 2013.

22. ANSYS® Academic Research Mechanical, Release 18.2, Help System, DesignXplorer Guide, ANSYS, Inc.